Testing Frontier Orbital Control: Kinetics of OH with Ethane, Propane, and Cyclopropane from 180 to 360K

James S. Clarke,* Jesse H. Kroll, Neil M. Donahue, and James G. Anderson

Department of Chemistry and Chemical Biology, Harvard University, Cambridge, Massachusetts 02138

Received: July 8, 1998; In Final Form: September 24, 1998

We test the hypothesis that the barrier to a gas-phase radical−molecule reaction is controlled by an avoided curve crossing of ground and ionic states of the reactants and products. We focus on the competing role of orbital overlap and energy difference on the delocalization energy of the transition state, comparing the reactions OH + ethane, OH + propane, and OH + cyclopropane using experimental data and theoretical analysis. These reactions constitute a homologous series in which the spatial extent and energy of interacting orbitals change dramatically, providing for an examination of the relative importance of energy and overlap on barrier height control. In addition, contrasting pictures of barrier height control, either by molecular properties or by bond properties of the reactants and products, are evaluated. Our kinetic data, obtained in a high-pressure flow system, cover a suppressed temperature range (180 − 360K) in order to isolate the lowest barrier pathway. The results for ethane and propane are consistent with barrier height control by the singly occupied molecular orbital (SOMO) of the OH radical and the highest occupied molecular orbital (HOMO) of the molecule. These are the historically defined frontier orbitals. The results for cyclopropane, however, suggest that it is the interaction of the SOMO with the second highest occupied molecular orbitals (SHOMOs) which controls barrier height. The SHOMOs of cyclopropane are spatially extended relative to the HOMOs; at the transition state the interaction between OH and the SHOMOs of cyclopropane overwhelms the interaction between OH and the HOMOs of cyclopropane. We examine the competition between energy and overlap of two reacting species and present an alternative definition of the frontier orbitals not necessarily as the highest energy orbitals, but rather as the orbitals that delocalize to the greatest extent at the transition state.

1. Introduction

Radical−molecule reactions control a wide range of chemical and biological systems, with reactivity ranging from immeasurably slow reactions to reactions that occur on every collision. Many radical−molecule reactions, atom-abstraction reactions in particular, are bimolecular in nature and have barriers associated with the transformation from reactant to product wave functions. Often this transformation may be described as a two-state avoided curve crossing.[1] Both the barrier height and barrier location are determined by the location of the minimum of the two-state crossing, modified by the configurational mixing of the two states. In strongly coupled systems such as those that we will consider here, the configurational mixing is substantial and the barrier height is greatly suppressed from the crossing energy.

Our understanding of these systems evolves from three areas: experimental observations, detailed ab initio studies, and mechanistic quantum-mechanical models. High-level, large basis-set theoretical calculations have made profound contributions to chemistry,[2,3] but these are practical for only relatively small systems. Moreover, the increasing complexity associated with larger systems can obscure the underlying controlling physics. Mechanistic quantum-mechanical models, stripped to the essential interactions and anchored in observed properties of the interacting species, serve to bind the experimental observations and ab initio calculations, thereby providing a more general chemical understanding. Our objective is to establish a framework for the accurate prediction of barrier heights given the physical properties of the separated reactants associated with the bonds or molecular orbitals participating in the reaction. In particular, we wish to determine if and how the properties of the separated species contribute to the energy and geometry of the transition-state complex.

In the simplest form of the two-state crossing model, the states that mix to form the reaction barrier are the ground and promoted states of the reactants and products, where the promoted state of the reactants maps to the ground state of the products and vice versa. A single interacting promoted state must be identified in both the reactants and products; usually this is assumed to be the lowest lying excited state of the appropriate symmetry. Possible excited states for a radical−molecule reaction include **(**1) the antibonding excited states of the bonds being broken or formed throughout the course of the reaction, **(**2) ionic states formed by removing an electron from a molecular orbital (MO) of the molecule and placing it into an MO of the radical, or **(**3) ionic states formed by removing an electron from an MO of the radical and placing it into an MO of the molecule. An excited state described by 1, however, is quite different from those described by 2 and 3, leading to two distinct perspectives on the mechanisms controlling reactions. These perspectives correspond to control by bond properties of the reactants and products (i.e., covalent control)[4,5] and control by molecular properties of the reactants and products (i.e., molecular control).[6,7]

In the covalent approach, the excited states are triplet states of the bonds being broken in the reactant and product molecules. For most systems, triplet excited states are directly related to the bond dissociation energy of the breaking bond.[8] Thus, a

10.1021/jp982922i CCC: $15.00
Published on Web 11/10/1998

tight relationship between the barrier height to reaction and the bond dissociation energy of the breaking bonds is expected within a homologous series of reactions. The covalent treatment of the two-state crossing model predicts similar trends to those predicted by theories in which barrier height is controlled by the enthalpy of reaction.[9−11]

In the molecular-orbital approach, frontier-orbital interactions generally determine the barrier heights and reaction rates in radical−molecule reactions.[12−15] A frontier-orbital treatment of an atom-transfer reaction is based upon the interaction of the frontier molecular orbital (FMO) of the molecule with the FMO of the radical. These are the highest occupied molecular orbital (HOMO) or lowest unoccupied molecular orbital (LUMO) of the molecule and the singly occupied molecular orbital (SOMO) of the radical. This two-orbital interaction plays the dominant role in the transfer of electron density from one species to the other during the course of a reaction.[16−18]

When the two-state crossing model is applied in this context, the excited states are described by the delocalization of electron density between the frontier orbitals of each species. When the degree of delocalization is large, each of the reacting species within the excited state is ionic in nature. Thus, the height of the reaction barrier is related to the ionization potential (IP) of the FMO of one species minus the electron affinity (EA) of the FMO of the other (IP−EA). The observed reactivity of a wide range of systems has been explained by trends in the IP or EA of either the reactant molecule or radical. These systems include the reactions OH + Cl_2, Br_2, and BrCl;[19] X + ClNO (X = Cl, F, Br, OH, O, N);[16] X + ClOCl (X = Cl, F, Br, OH, O, N);[18] and the general class of H atom abstractions from alkanes by a series of radicals.[6]

While the two-state crossing model is conceptually powerful, it is a considerable oversimplification. There are at least two factors which complicate this simple picture. First, the dominant state may not always be the lowest energy state of appropriate symmetry. In this event, the two-state model can be preserved by identifying the appropriate excited state and continuing to assume that other states play a negligible role in the reaction. Second, multiple states may participate in the transition-state configuration interaction. In this event, the two-state model can still be useful if a weighted anchor point, or virtual excited state, can be identified. In this paper we explore the effects of these complicating factors. First, we show that a series of hydrogen atom transfers are better described by the molecular properties of the reactants and products (i.e., ionization potential, electron affinity, molecular polarizability, etc.) than by the bond properties of the reactants and products (i.e., bond dissociation energy, bond dipole moment, etc.). Second, we show that the interaction between a pair of FMOs cannot always adequately describe the delocalization of electron density taking place throughout the course of a reaction. In particular, we examine the sometimes competing role of molecular overlap and energy difference in the coupling between various excited states and the ground state. Using these observations, we endeavor to gain greater insight into how the molecular properties of the reactants and products control both barrier height and barrier location in radical−molecule reactions.

To anchor this evaluation we present experimentally determined thermal rate constants of OH + cyclopropane, OH + propane, and OH + ethane measured over a wide temperature range (180−360 K). We also use observed bond and molecular properties of reactants and products, augmented by low level ab initio calculations when necessary, to constrain the boundary conditions of these crossing models. We then investigate this series of reactions theoretically, examining the explicit competition between energy and overlap of two reacting species. Our results indicate that spatially extended but energetically stable orbitals can determine the site of radical attack. This forces us to redefine the frontier orbital in terms of the potential for electron delocalization rather than differences in orbital energy.

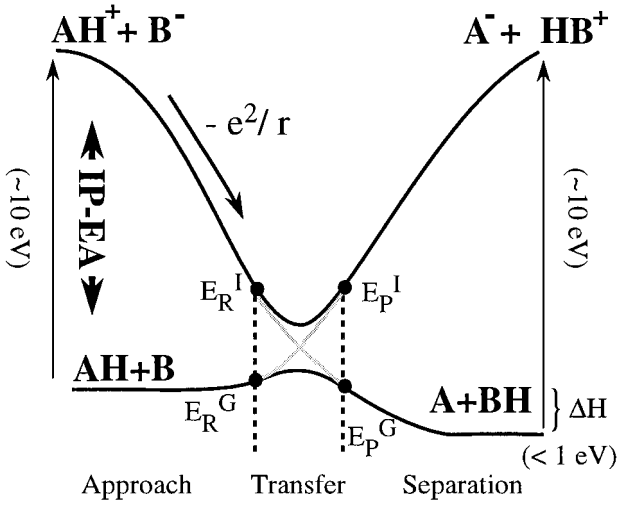

Figure 1. An atom-transfer reaction in the context of the ionic curve-crossing model. The reaction coordinate is separated into three stages. The energies of reactants and products on the ground state at the beginning and end of the transfer stage are given by E_R^G and E_P^G, while the energies of the reactants and products on the ionic surfaces at the beginning and end of the transfer stage are given by E_R^I and E_P^I. Note the height of the ionic surface (∼10 eV) in comparison to the barrier to reaction (∼0.1 eV) and the enthalpy of reaction (∼1 eV).

2. Background

We shall briefly describe the ionic and covalent theories of barrier height control as they apply to radical−molecule reactivity. Both are discussed in much greater detail in Donahue et al.[6] and references therein.

2.1. Ionic Curve Crossing. We have recently presented a theory describing barrier height control by an ionic curve crossing.[6,7] Figure 1 shows the reaction scheme for a simple hydrogen atom abstraction. We model the evolution of two states along the reaction coordinate: the ground state and an excited ionic state. The ionic state is formed by removing an electron from the HOMO of the molecule and inserting it into the SOMO of the radical. The reaction coordinate is broken into three stages using different approximations to analyze the evolution of each state. In the first stage, the reactants approach each other and Coulombic interactions dominate. In the second stage, the two states cross as the atom transfer is executed. Here the configuration interaction controls the energies. In the third stage, the products separate and Coulombic energies again dominate.

The first stage describes the approach of the undistorted reactants. In this stage, the ground state energy often decreases slightly due to long-range forces, then ultimately increases as reactant orbitals begin to develop overlap. The ionic-state energy is initially greater than the ground-state energy by approximately IP of the molecule minus EA of the radical; however, the energy drops dramatically as the reactants approach, due to the electrostatic attraction between the two virtual ions. To zero order, the height of the ionic surface, E_R^I, at the

end of the approach stage is given by

$$E_R^I \cong IP_{HOMO} - EA_{SOMO} - \frac{e^2}{r} \quad (1)$$

Higher order terms may be calculated[6,20] which include the effects of reactant dipole moments and reactant polarizability.

The third stage is conceptually identical to the first, with the ground and ionic surfaces offset by the reaction enthalpy. It is important to note that the energies of the excited surfaces are much greater than the enthalpy of reaction, so that enthalpy plays only a small role in determining the barrier height. Together, the first and third stages establish the boundary conditions for an avoided curve crossing in the second stage.

The second stage is characterized by the onset of overlap between the two reactants, the delocalization of electron density from the HOMO of the molecule to the SOMO of the radical, and the associated movement of an H atom from one species to another. We model this stage as a three-electron problem; as the ground and ionic states mix, two electrons in the A−H bond delocalize with the one electron in the SOMO of the radical B. This results in a two-state configuration interaction which lowers the barrier and loosens the transition state. An increase in the propensity for electron delocalization, or polarizability of the reactants near the TS, causes a greater degree of configurational mixing and suppresses the barrier further.

We assume that the unperturbed energies evolve linearly during the curve crossing as the H atom moves along the A−H−B coordinate. The height of the crossing point E_X during the atom-transfer stage can be derived in this simple model and is given by

$$E_X = E_R^G + \frac{(E_R^I - E_R^G)(E_P^I - E_P^G + \Delta H_{rxn})}{(E_R^I - E_R^G) + (E_P^I - E_P^G)} \quad (2)$$

where E_R^G and E_R^I are the energies of the ground and ionic surfaces at the beginning atom transfer stage, and E_P^G and E_P^I are the energies of the ground and ionic states at the end of the atom transfer stage.[6] Equation 2 shows that the height of the barrier crossing is primarily determined by the geometric mean of the energy gaps for the reactants and products and the degree of electron delocalization at the transition state.

Simple geometry also allows one to predict the location of the crossing. Equation 3 gives the fractional position ρ_{TS}/R_X along the A−H−B coordinate

$$\frac{\rho_{TS}}{R_X} = \frac{(E_R^I - E_R^G) - (E_P^I - E_P^G)}{(E_R^I - E_R^G) + (E_P^I - E_P^G)} \quad (3)$$

where $2R_X$ is the total distance the H traverses in moving from reaction center A to reaction center B, and ρ_{TS} is the distance from the transition state to the point R_X.[7] Thus, ρ_{TS}/R_X can have values between −1 and 1, where 0 represents a symmetrical reaction. The position of the barrier is determined by the relative sizes of the reactant and product energy gaps.

Finally, the transition-state R−X distance, the distance of the minimum crossing height, is determined by a balance of energy gradients on the ground and ionic surfaces,[7]

$$e^2/r^2 = -2\ \partial E^\sigma/\delta r \quad (4)$$

where E^σ is the coulomb and exchange repulsion encountered along the diabatic, undistorted approach coordinate (stage 1). This term is proportional to the orbital overlap between the reactants. We thus expect a systematic relationship between the spatial extent of the reactant orbitals and the transition state location.

Ground-State Energies. We separate the ground-state energy into two components: the short-range Coulomb-exchange repulsion term E^σ, discussed above, and a long-range dipole−dipole term E^μ, due to the charge distribution on the reactants.[7] The total ground-state energy is thus

$$E^G = E^\mu + E^\sigma \quad (5)$$

The long-range term may be approximated as

$$E^\mu \sum^m \sum^n \frac{\delta_m \delta_n}{r_{mn}} \quad (6)$$

where δ represents the partial charge on a particular atom, r_{mn} is the internuclear distance between two atoms, and m and n are the atoms of molecules AH and B (or A and BH), respectively. Because the barrier is formed at a small and relatively constant value of the repulsive term E^σ, the predominant term in the ground-state energy is E^μ.

Since the systems under investigation here are strongly coupled, the barrier height E_b is given by

$$E_b = E^G + (1 - \beta)(E_X - E^G) \quad (7)$$

where β is a measure of the coupling strength between the two reactants. For a series of hydrogen abstractions from alkanes, we assume that β will not change dramatically from one reaction to another. Thus, we expect a linear relationship between the crossing height E_X and the quantity $E_b - E^G$, which is approximately $E_b - E^\mu$ at the end of stage 1.

2.2. Covalent Curve Crossing. Radical−molecule reactions may also be described by a two-state crossing theory in which the excited states are covalent.[4,5,21] For atom-transfer reactions, the excited states correspond to the singlet and triplet states of the reactant and product molecules, when the reactants are far apart. Along the reaction coordinate, the antibonding triplet (excited) state of the breaking bond maps with the radical doublet state into the product singlet (ground) state of the newly formed molecule. The energy difference between the ground and excited states ΔE, has been shown to be roughly

$$\Delta E = 0.75 \frac{5 - \Delta}{2(1 + \Delta)} D_0 \quad (8)$$

where Δ is a Sato or overlap parameter and D_0 is the bond strength of either the breaking bond of the reactants or forming bond of the products.[8,23] For $\Delta \simeq 0.2$, this energy gap becomes 1.5 D_0. In this theory, the crossing height of the excited states can be derived to give[5,6]

$$E_X = \frac{(D_{0R} + 0.5 D_{0P})}{1 + D_{0P}/D_{0R}} \quad (9)$$

where D_{0R} and D_{0P} are the strengths of the bonds broken and formed in the reaction. In eq 9, the curve crossing height depends primarily on the bond strength of the reactant.

3. Connecting Theory and Experiment

To explore the role of changing molecular properties, we consider a series of OH + alkane reactions (methane, ethane, propane, and cyclopropane). This series of H atom abstractions presents an increasingly dense set of interacting MOs, culminat-

ing with cyclopropane, for which the dominant MO interaction may not be the HOMO−SOMO interaction. The molecular orbital description of cyclopropane is distinctly different from that of other alkanes;[24] the HOMOs of cyclopropane are not localized on the hydrogens but are instead associated with the highly strained carbon ring. Thus, when OH abstracts a hydrogen from cyclopropane, these orbitals may not play the dominant role in the reaction. Furthermore, for most alkanes, the C−H bond dissociation energy scales with the ionization potential of the frontier orbital, the HOMO. This is not the case with cyclopropane. The ionization potential of the HOMO of cyclopropane is lower than that of most other alkanes, while the bond dissociation energy of the C−H bond in cyclopropane is greater than that of any other alkane. This allows for a direct comparison of the predictive capability of a theory that uses molecular properties and a theory that uses bond properties. Measurements of these rates at low temperatures allow precise determinations of the activation energies and the preexponential factors under conditions where one pathway dominates each reaction. The kinetics of OH + methane are well established;[25] thus, we will focus on the measurements of OH with ethane, propane, and cyclopropane.

4. Experimental Method

The high-pressure flow system (HPFS) and analysis methods used in this work are described extensively in the literature[26,27] but will be summarized here along with changes specific to this work.

The HPFS consists of a 700 L settling chamber connected to a 10 m long, 12.36 cm diameter stainless steel pipe containing a well-developed flow of nitrogen gas. System pressure is measured with a calibrated 1000 Torr capacitance manometer (MKS). Velocity is measured with a pitot-static tube located in the center of the flow and connected to a 1 Torr differential capacitance manometer (MKS). The mass flow of nitrogen is held constant throughout the experiments, resulting in a velocity of 10−15 m/s, depending on the temperature of the system. Temperature is measured in the center of the flow tube at the beginning and end of the reaction zone. Measurements are made under pseudo-first-order conditions with the hydrocarbon as the excess reagent (XS).

Hydroxyl radicals are produced in a sidearm source from the fast titration reaction $H + NO_2 \rightarrow OH + NO$ in excess NO_2 and then injected into the center of the carrier flow. Hydroxyl radicals are detected via laser induced fluorescence (LIF) at five equally spaced detection axes.

This experiment differs from previous experiments performed on our HPFS in that the carrier gas no longer recirculates. This allows us to establish several discrete, steady-state XS concentrations in rapid succession instead of slowly varying the XS concentration with dilution. By modulating the XS concentration we reduce our sensitivity to experimental drifts. Hydroxyl radical fluorescence is monitored while the XS reagent is cycled on and off at the various concentrations.

Excess reagent concentrations are measured via FTIR absorption spectrometry in a 44-pass White cell situated between the first two LIF axes. Spectra obtained with no XS in the system serve as a background. The ratios of signal to background are transmittance spectra, which we analyze for the XS concentration using a correlation algorithm.[28] Because our White cell mirrors are recessed and purged from the actual flow, we calibrate our path length using halocarbon F12, whose IR spectrum is well established.[29]

Sensitivity to both OH decay and XS reagent detection is optimized by adjusting the cycling time. This allows for the variation of both the number of XS reagent concentrations measured and the experimental time scale. We currently choose six XS reagent concentrations per rate measurement, resulting in an experiment length of 300−600 s.

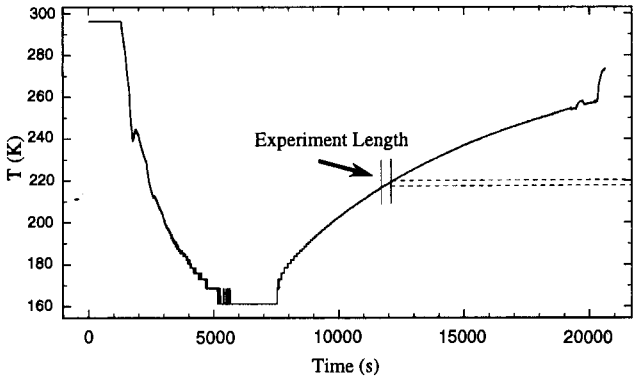

Figure 2. System temperature versus time, measured at the radical source. LN2 is injected at a rate of 10 g/s from $t = 1200$ to $t = 7500$. Our temperature reading goes off-scale at approximately 160 K. At $t = 7500$, the LN2 is turned off in exchange for N_2 gas. The time scale and temperature profile of a single experiment are shown.

We heat the HPFS with resistive heating tape wrapped externally around the HPFS, which is also covered with high-grade insulation (TechLite). The heaters can provide up to 2 kW of heat directly to the wall of the tube, warming the carrier gas as it proceeds toward the detection zone. Measurements are quickly repeated as the system warms at a rate of 10−15 K/h, such that the temperature increase during the course of the run is small. Temperatures of 360 K can be achieved, and the temperature can be cycled several times in a single day to allow for many runs.

We cool the HPFS internally with a steady stream of liquid nitrogen (LN2). The LN2 is injected through a vacuum-jacketed tube inserted into the settling chamber of the HPFS, and is regulated by a cryogenic liquid control valve (Worcester Control). We allow about 2 h for cooling, consuming close to 100 L of LN2. Once the system reaches its lowest temperature, the LN2 flow is replaced by a 50 slm flow of room-temperature N_2. The N_2 gas quickly cools as it flows down the system. The entire system warms with a thermal time constant of 2 h, producing the temperature profile illustrated in Figure 2. Once the N_2 carrier flow is turned on, measurements are made as the system warms. Both axial and radial temperature gradients in the detection axis are small. At the coldest temperatures, however, these gradients limit our accuracy to ±10%. Over the course of a run, the system warms no more than 3−5° at the coldest temperatures. With this method, the HPFS is routinely capable of measurements at 190 K.

4.1. Materials. A liquid nitrogen boil-off source is used without further purification for the HPFS carrier flow. The liquid nitrogen for cooling is used without further purification from a liquid nitrogen gas pack (Middlesex Welding). Mixtures of 2% hydrogen gas in UHP helium (Matheson), and 2% NO_2 gas in UHP helium (Matheson) are used in the OH source. Ethane (Scott), propane (Aldrich), and cyclopropane (Aldrich) are used as received after FTIR analyses showed no substantial amounts of contaminants.

5. Experimental Results

Data for the three reactions are presented in Table 1. Experiments were performed in rapid succession as the system warmed, either from low temperatures to room temperature or from room temperature to elevated temperatures.

TABLE 1: Averaged Rate Data and Number of Individual Measurements for the Reactions of Ethane, Propane, and Cyclopropane with OH at Various Temperatures

temperature (K)	no.	k(ethane + OH) (10^{-13} cm^3 s^{-1})	no.	k(propane + OH) (10^{13} cm^3 s^{-1})	no.	k(cyclopropane + OH) (10^{-13} cm^3 s^{-1})
180	1	0.269 ± 0.027				
190	3	0.377 ± 0.004	3	3.626 ± 0.247		
200	6	0.454 ± 0.025	7	4.136 ± 0.127	2	0.212 ± 0.043
213	7	0.651 ± 0.007	6	4.864 ± 0.095	3	0.296 ± 0.017
225	5	0.808 ± 0.012	4	5.602 ± 0.063	2	0.347 ± 0.004
238	6	0.967 ± 0.018	5	6.475 ± 0.053	7	0.378 ± 0.004
250	8	1.251 ± 0.014	7	7.532 ± 0.051	4	0.426 ± 0.004
265	8	1.640 ± 0.018	5	8.691 ± 0.147	5	0.515 ± 0.013
280	3	2.081 ± 0.016			3	0.591 ± 0.007
295	21	2.515 ± 0.021	12	11.29 ± 0.159	17	0.657 ± 0.008
310	3	2.953 ± 0.050	5	12.76 ± 0.182	5	0.752 ± 0.012
325	5	3.464 ± 0.037	4	13.56 ± 0.140	4	0.897 ± 0.024
340	2	3.744 ± 0.038	3	14.80 ± 0.136	2	1.009 ± 0.002
360	6	4.637 ± 0.164	5	16.40 ± 0.229	1	1.161 ± 0.075

All data sets were fit to a modified Arrhenius expression.[30] This accounts for the curvature in Arrhenius plots caused by the conversion of rotational modes of the individual reactants to loose vibrational modes of the transition state. For each of the reactions under investigation here, the following expression is used:

$$k(T) = \frac{B e^{(-E_a/T)}}{T\,(1 - e^{(-1.44\nu_1/T)})^2\,(1 - e^{(-1.44\nu_2/T)})} \qquad (10)$$

Values for ν_1 and ν_2 are taken taken to be 280 and 500 cm^{-1}. Tunneling is neglected. While it is expected that ν_1 and ν_2 will vary somewhat from reaction to reaction, the choice of these values allows the temperature dependence in the preexponential to be modeled explicitly.

To present a manageable data set, we use the fit results to interpolate each measurement to the closest of 14 reference temperatures, then average the data at each temperature. These are the values shown in Table 1. The precision of the measurements at each of the temperatures are also given. The accuracy of our data is ±5% (1σ) within 50 K of room temperature and ±10% outside this range.

5.1. Ethane + OH → Products. We measured the rate constants for the reaction of ethane + OH a total of 84 times over the temperature range 180−360 K. OH decay was linear over nearly 2 orders of magnitude after subtraction of laser scatter. Figure 3 shows the Arrhenius plot for this reaction including data from this study as well as other major studies. A least-squares analysis of the combined data sets gives

$$k^{298} = (2.52 \pm 0.12) \times 10^{-13}\ \text{cm}^3\ \text{molecule}^{-1}\ \text{s}^{-1} \qquad (11)$$

and

$$k(T) = \frac{(1.16 \pm 0.03 \times 10^{-9})\, e^{(-1023 \pm 7/T)}}{T\,(1 - e^{(-1.44(280/T))})^2\,(1 - e^{(-1.44(500/T))})} \qquad (12)$$

over the temperature range 180−500 K. Our rates are in excellent agreement with other published measurements, including those taken previously in this laboratory,[30] over the full temperature range; however, the difference in shape between the common Arrhenius function ($CT^n e^{-D/T}$) and the modified form is evident in the residuals.[25]

5.2. Propane + OH → Products. We measured the rate for the reaction of propane + OH a total of 66 times over the temperature range 190−360 K. Again, OH decays were linear. Figure 4 shows the Arrhenius plot for this reaction including data from this study as well as other major studies. A least-squares analysis of the combined data sets gives

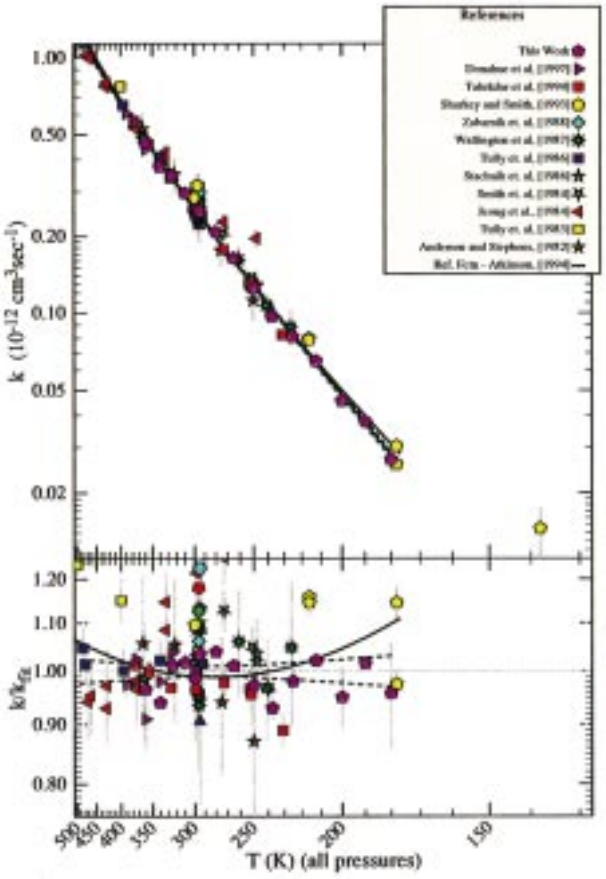

Figure 3. Rate constant, k, vs T for the reaction of ethane + OH → products. The temperature-dependent studies are indicated in the legend. Error bars for individual measurements are shown. The ratios of the data to the modified Arrhenius fit are shown in the residual plot at the bottom. The uncertainty of this overall fit is shown by the dotted lines on the graph and residual plot. The recommendation of Atkinson is also shown.[35]

$$k^{298} = (1.12 \pm 0.06) \times 10^{-12}\ \text{cm}^3\ \text{molecule}^{-1}\ \text{s}^{-1} \qquad (13)$$

and

$$k(T) = \frac{(1.31 \pm 0.03 \times 10^{-9})\, e^{(-615 \pm 6/T)}}{T\,(1 - e^{(-1.44(280/T))})^2\,(1 - e^{(-1.44(500/T))})} \qquad (14)$$

over the temperature range 190−400 K.

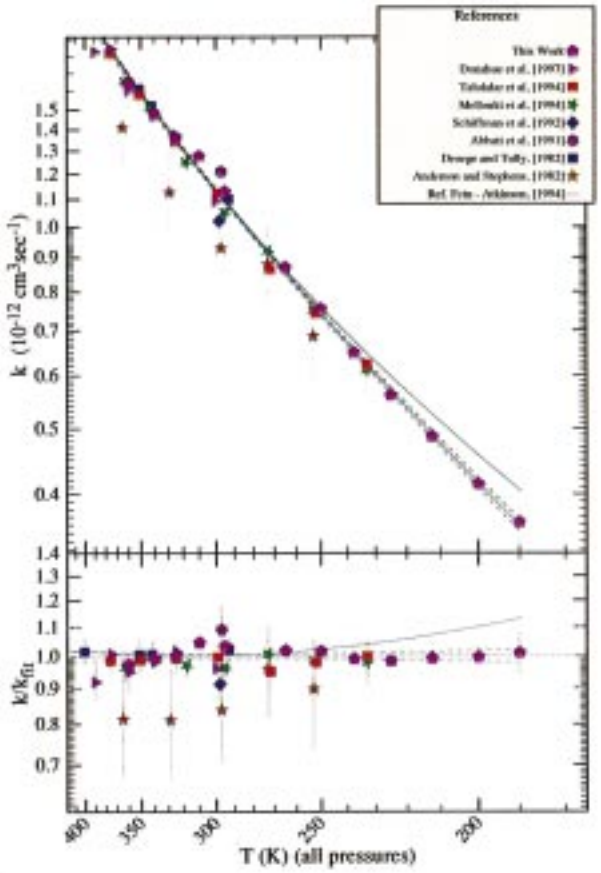

Figure 4. Rate constant, k, vs T for the reaction of propane + OH → products. The temperature-dependent studies are indicated in the legend. Error bars for individual measurements are shown. The uncertainty of this overall fit is shown by the dotted lines on the graph and residual plot. The ratios of the data to the modified Arrhenius fit are shown in the bottom panel. The recommendation of Atkinson is also shown.[35]

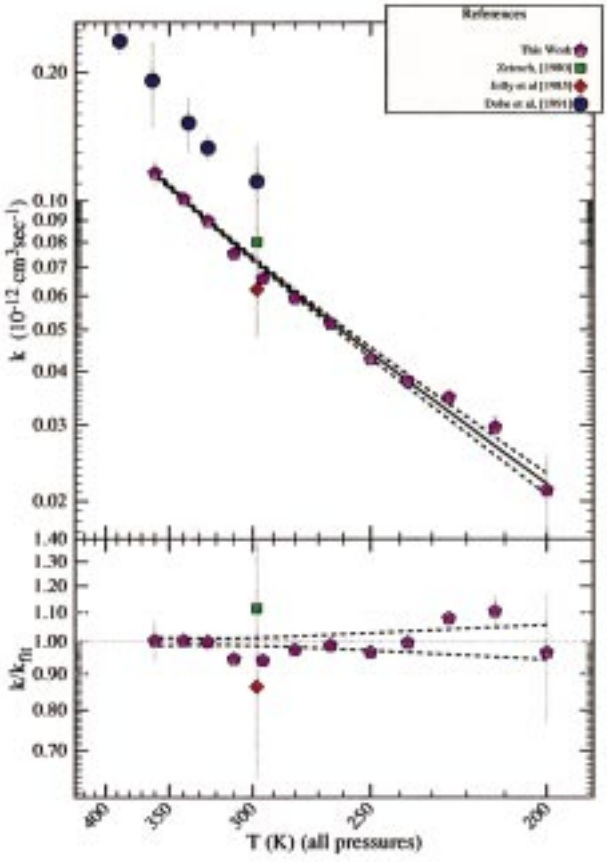

Figure 5. Rate constant, k, vs T for the reaction of cyclopropane + OH → products. The studies are indicated in the legend. Error bars for individual measurements are shown. The ratios of the data to the modified Arrhenius fit are shown in the bottom panel. The uncertainty of this overall fit is shown by the dotted lines on the graph and residual plot.

Our rates are in excellent agreement with existing measurements down to 233 K.[25] We extend the range of measurements down to 190 K. In this region, the kinetics continue to show Arrhenius behavior. This is consistent with the expectation that at lower temperatures only one reaction pathway (abstraction of the secondary hydrogens) is significant.

5.3. Cyclopropane + OH → Products. We measured the rate for the reaction of cyclopropane + OH a total of 55 times over the temperature range 200−360 K. A small amount of OH regeneration was observed in the reaction zone during the course of the reaction. It is likely that HO_2 is produced rapidly in the oxidation reactions following the initial reaction with OH. This HO_2 reacts quickly with NO from the radical source to regenerate OH. To account for this, only the initial slopes of the decay plots were used to determine the rate constant.

The results of these measurements are shown in Figure 5. A least-squares analysis of only our data set gives

$$k^{298} = (6.49 \pm 0.46) \times 10^{-14}\ \text{cm}^3\ \text{molecule}^{-1}\ \text{s}^{-1} \quad (15)$$

and

$$k(T) = \frac{(1.25 \pm 0.06\ 10^{-10})\ \text{e}^{(-733 \pm 14/T)}}{T\,(1 - \text{e}^{(-1.44(280/T))})^2\,(1 - \text{e}^{(-1.44(500/T))})} \quad (16)$$

over the temperature range 200−360 K. While the data at 213 and 225 K are high with respect to the residual, they are both within the accuracy range that we claim for our measurements at these temperatures. In comparison to the reaction of OH with propane, the activation energy is slightly higher, while the preexponential is an order of magnitude lower.

Data from other major studies of this reaction are also shown in Figure 5. The three previous studies on the reaction of OH + cyclopropane are Dóbé et al.,[31] Jolly et al.,[32] and Zetsch.[33] The room-temperature rates vary by 80% over the full range.

Mechanism. To investigate possible causes of this discrepancy, we performed a reaction modulation spectroscopy (RMS) product study experiment similar to that described by Donahue et al.[28] The OH radical source was cycled on and off with a 5 min duty cycle by modulating the hydrogen gas flow through the radical source. This allowed the measurement of the concentration and identities of the reactants and products with high sensitivity. The initial OH concentration was 1×10^{12} molecules cm^{-3}, while the initial cyclopropane concentration was 5×10^{14} molecules cm^{-3}. In addition, the NO_2 and O_2 were present at concentrations of 7×10^{12} and 4×10^{14} molecules cm^{-3}, respectively. Initial results indicate that, with sufficient NO (from NO_2) present, formaldehyde and CO are produced in high yield (24% and 35% of the total carbon budget, respectively) by the rapid decomposition of radical intermediates derived from cyclopropane. Ethene is produced in much lesser quantities (9% of the total carbon budget). We expect formaldehyde and the formyl radical to be the dominant products in an abstraction pathway. Formaldehyde quickly reacts with OH ($k = 1.0 \times 10^{-11}$ cm^3 molecules^{-1} s^{-1})[34] to produce H_2O and

the formyl radical, which will quickly decompose in the presence of O_2 to form CO and HO_2. Unlike straight-chained alkanes, cyclopropane has the possibility of a ring opening caused by the addition of OH. From this pathway, we expect ethene to be the primary product of an OH addition pathway, although ethene production from the abstraction pathway is also possible. This is similar to the decomposition mechanism for OH-olefin oxidation, which has been previously documented.[28]

We have also located abstraction and addition transition states with ab initio calculations (UMP2/6-31G**). The abstraction pathway has a barrier of 0.43 eV, while the addition pathway has a barrier of 1.06 eV. While these values are not quantitatively accurate, they do indicate that the addition pathway is significantly higher in energy than the abstraction pathway and therefore does not likely play a significant role in the reaction between cyclopropane and OH.

The study by Dóbé et al. was performed with a laser flash photolysis/resonance fluorescence technique. Hydroxyl radicals were produced in large concentrations (1×10^{12} molecules cm^{-3}) by photolyzing nitric acid at 193 nm. At this wavelength, the nitric acid photolysis inevitably produced high quantities of NO_x (NO and NO_2). The large amount of formaldehyde subsequently produced would therefore bias the measured rate constant, leading to an overestimation of the rate by as much as a factor of 2.

In contrast, the study by Jolly et al. used water vapor as the photolyte to produce OH. Under these conditions, formaldehyde formation would be suppressed. Our room-temperature rate is in reasonable agreement with this study. The work of Zetsch was a private communication to Atkinson[35] and cannot be reviewed.

Formaldehyde production did not significantly influence our kinetics measurements. In all measurements, the initial OH concentration was kept below 1×10^{10} molecules cm^{-3}; in addition, NO_x concentrations were minimized. Under these conditions, the formaldehyde−OH reaction would account for no more than 0.2% of the total OH decay. It is possible to manipulate our experimental conditions such that significant regeneration occurs ([OH] = 5×10^{11} molecules cm^{-3} and [NO_2] = 1×10^{12} molecules cm^{-3}). Under these conditions, we observe elevated rates as well.

6. Discussion

We can now compare the ionic and covalent curve crossing models as a test of barrier height control by molecular properties versus bond properties. This is accomplished by comparing predicted curve-crossing heights with experimentally measured barriers for a series of OH−alkane reactions, including OH + cyclopropane. In Figure 6 we show results for both models. This is similar to the comparison shown in Donahue et al.,[6] with two major differences: we show only OH reactions, and we include an explicit treatment of the ground-state energy. The experimental activation energies (E_a), calculated ground-state dipole energies (E^μ), and their differences are shown in Table 2. We use measured ionization potentials, electron affinities[36] and bond strengths[37] to calculate the ionic and covalent crossing heights (eqs 2 and 9, respectively). We also use low-level ab initio calculations (UHF/6-31G**) to constrain the transition state distance and calculate charge distributions for the long-range ground-state energy E^μ (Eq 6). Data for the reaction of OH + methane are from Atkinson[25] and DeMore et al.,[34] while data for the additional compounds are from Donahue et al.[30]

The analysis of other radical−alkane reactions presented in Donahue et al.,[6] which includes a large set of radicals but not cyclopropane, provides strong evidence that the ionic curve crossing model consistently describes radical−molecule reactivity. We note two important points of that study: (1) There exists a tight correlation between ionization potential (IP) and bond dissociation enthalpy (D_0) for most hydrocarbons. Thus,

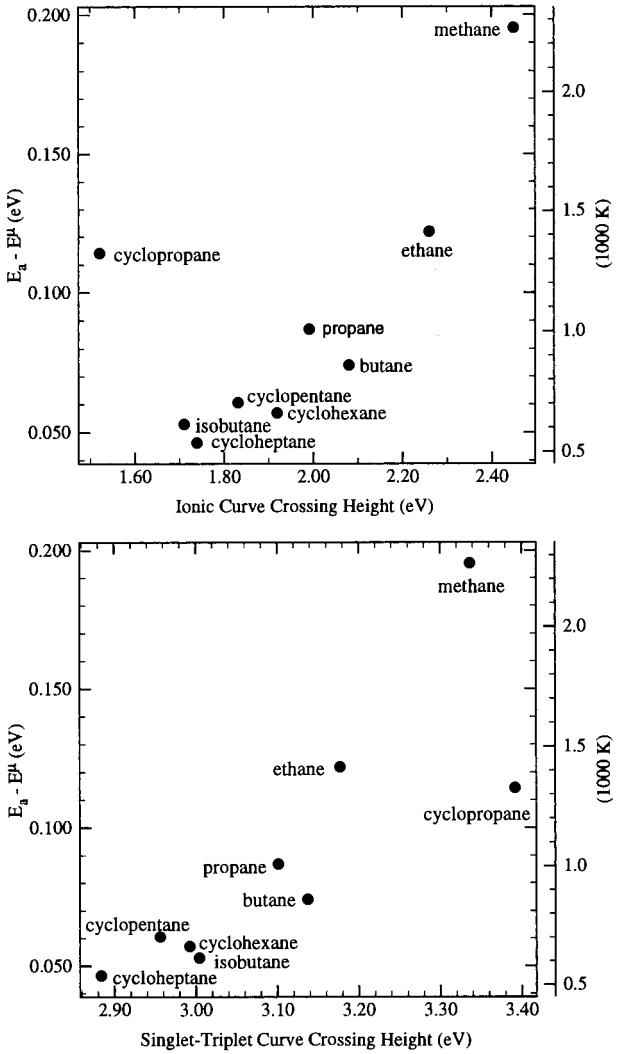

Figure 6. Activation energy (minus ground-state energy) versus ionic crossing height (top) and covalent crossing height (bottom) for a series of H atom abstractions from alkanes and cycloalkanes. The reaction of cyclopropane with OH lies well outside the correlation among the other reactions for both theories. The ionic crossing theory underpredicts the activation energy, while the covalent crossing theory overpredicts the activation energy.

TABLE 2: Activation Energies (E_a), Ground-State Dipole Attraction Energies (E^μ), and Dipole-Corrected Barrier Heights ($E_a - E^\mu$) for a Series of Hydrocarbons[a]

compound	E_a (K)	E^μ (K)	$E_a - E^\mu$ (K)
methane[b]	1860	−408	2268
ethane[c]	1026	−385	1411
propane[c]	616	−394	1010
isobutane[d]	257	−357	614
butane[d]	454	−405	859
cyclopentane[d]	253	−452	705
cyclohexane[d]	227	−434	661
cycloheptane[d]	256	−280	536
cyclopropane[e]	735	−588	1323

[a] The dipole energies were computed from eq 6 using results from theoretical calculations (UHF/6-31G**). [b] Data from Atkinson[25] refitted from eq 10. [c] Present work. All data sets taken together. [d] Data from Donahue et al.[30] [e] Present work. Our data set only.

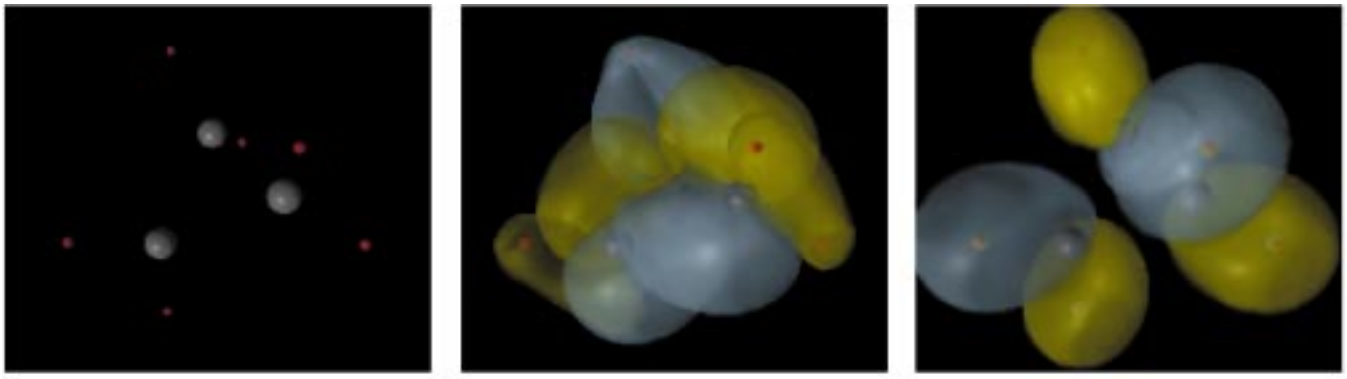

Figure 7. Structures and orbitals from ab initio calculations (UMP2/6-31G**) representing the structure and electron distribution of cyclopropane. The gold and silver colors correspond to wave functions of the opposite sign. Bare structure (left), two degenerate HOMOs (center), and two degenerate SHOMOs of cyclopropane (right) are shown. Spatially, the SHOMO extends further than the HOMO.

both the ionic and covalent models of reactivity will give similar reactivity trends for a single radical with a series of molecules. (2) There is no single correlation between electron affinity (EA) and bond dissociation enthalpy (D_0). When examining the reactions of a single molecule with a series of radicals, the ionic curve-crossing model predicts reactivity far more successfully than the covalent model. However, neither model presented in Figure 6 appears to predict the cyclopropane−OH barrier. In both cases measured barriers increase consistently with crossing height for the other molecules, but the cyclopropane barrier is underpredicted by the ionic curve crossing model and overpredicted by the covalent model. We must therefore consider higher order contributions in either case if this reaction is to be understood.

To first order, the parameter that can vary in the covalent curve crossing model is Δ, the Sato or overlap parameter. Raising this parameter lowers the singlet−triplet energy gap and hence lowers the barrier. While the explicit calculation of this parameter for cyclopropane is beyond the scope of this paper, we do not expect Δ to be higher than in other hydrocarbons. The greater stability of the C−H bond partially compensates for the ring strain of the cyclopropane carbon skeleton.[38] Thus, any delocalization of electron density from this bond in the course of a reaction also destabilizes the cyclopropyl group. If anything, we expect the singlet−triplet energy gap to be larger for cyclopropane than for nonstrained hydrocarbons. Thus, we expect the covalent crossing would be higher for the cyclopropane OH reaction, exacerbating the disagreement with observations shown in Figure 6.

There are two aspects of the ionic curve crossing model requiring attention. The first is the low level of theory used to constrain the barrier location and calculate the ground state energy. The second is the oversimplification of treating only a single configuration in the two-state model. Up to this point, we have assumed that only one molecular orbital of the molecule, the HOMO, plays a significant role in the reaction. In the full configuration interaction, all of the orbitals of cyclopropane are considered. It is important to view the reaction from the point of view of the radical: From which molecular orbital or orbitals does the OH withdraw electron density? Since ionization potential is a molecular orbital property, we can explicitly treat the role of multiple orbitals in the general context of the ionic crossing problem.

To further investigate the role of multiple orbitals in the context of our theory, we focus on the reactions of OH with methane, ethane, propane, and cyclopropane. Limiting our study to the smaller species allows us to include electron correlation by using the more accurate UMP2/6-31G** level of theory.

6.1. Theoretical Results. We performed ab initio calculations (UMP2/6-31G**) on the reactions of OH with methane, ethane, propane, and cyclopropane, optimizing reactants, products, and transition states. For each of the above reactions, we have analyzed the wave functions for each of the molecular orbitals (MOs). The shapes and relative energies of the orbitals (which indicate the preferred sites of OH attack) do not differ from those calculated with the UHF/6-31G** level of theory. Also, simply changing the level of theory does not sufficiently change the interaction distance for any of the reactions to alter the appearance of Figure 6. The low level of theory used previously therefore does not explain the cyclopropane anomaly. Orbital overlap calculations (Figure 7), however, do reveal a difference in cyclopropane.

In methane and ethane, significant electron density surrounds each of the hydrogens in the HOMOs. The SOMO of the attacking OH radical (a half-filled p-orbital) will therefore overlap substantially with any of the hydrogens, leading to a stable transition state. In propane, a significant amount of electron density is concentrated on the secondary hydrogens, with less density on the primary hydrogens, thus favoring abstraction from a secondary hydrogen. This result is consistent with the findings of Hu et al.[39] Cyclopropane (Figure 7), in contrast, has relatively little electron density around the hydrogens in the two degenerate HOMOs. Instead, the electron density is focused in the carbon ring structure. The second highest occupied molecular orbitals (SHOMOs) have the greatest amount of electron density around the hydrogens. The SHOMOs are spatially extended but far more stable (2.5 eV lower) than the HOMOs. Thus there is a competition between energy and overlap; the SOMO of the OH radical overlaps with the SHOMOs before overlapping with the HOMOs despite their more stable energy.

6.2. Delocalization. The appeal of a two-state model is its conceptual simplicity and the ability it gives us to explore the influence of various phenomena on both the curve-crossing height and the barrier height. We wish to retain this framework by adding additional configurations in a perturbative manner. To do this, we must identify the zeroth order and higher order interactions. The appropriate state to choose as the boundary condition to the curve-crossing problem at zeroth order is the state with the largest coupling to the ground state. Assuming that the coupling strength is constant throughout the atom-transfer stage of the reaction, we can begin to calculate these coupling terms using the expressions derived by Fukui and Fujimoto.[40,41] The essential conclusion is that the coupling strength or delocalization is proportional to the square of the

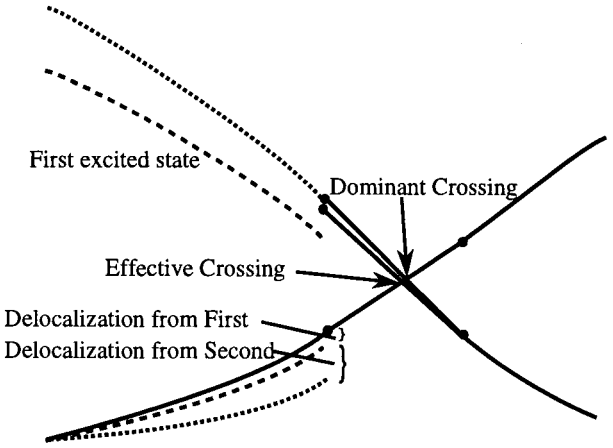

Figure 8. The competition between energy and overlap. The second excited state is higher in energy than the first, but the greater overlap between second excited state and the ground state overwhelms the higher energy. This becomes the dominant state in the configuration interaction and gives the appropriate boundary condition for the curve crossing problem. Still, the first excited state plays a minor role. Weighting this appropriately leads to an effective boundary condition to the two-state curve-crossing problem.

overlap between the ground and excited states divided by the energy of the excited state.

In cyclopropane there are two candidates for the zeroth-order configuration: the HOMO, which has lower energy, and the SHOMO, which has larger overlap with the SOMO of OH. When two excited states dominate the configuration interaction for the reaction, and one state is higher in energy but has greater overlap (see Figure 8), it is entirely possible that the overlap might outweigh the difference in energy between the states. If the greater coupling strength between the higher energy excited state and the ground state continues throughout the reaction, then these states determine the simple crossing point.

However, the actual barrier is a result of the full configuration interaction. In Figure 8, the first excited state further suppresses the barrier to reaction. In the context of the two-state crossing model, this first excited state lowers the effective energy of the boundary condition by the weighted difference between the coupling strengths.

To specifically quantify the role of each MO in determining the magnitude of electron delocalization and hence barrier suppression, an expression giving the relative extent that a molecular orbital delocalizes during the early stage of a reaction was derived. The dominant configuration interaction in hydrogen atom abstractions is the transfer of an electron from an orbital of the hydrocarbon to the SOMO of the radical. Using the method of Fukui and Fujimoto, this may be treated as a perturbation on the ground-state interaction of the undistorted, separated species. A secular determinant can be solved to show that the transfer of electron density, or delocalization (D), decreases the energy by

$$D = \sum^{\text{Occ MOs}} \frac{(H_{0,\text{MO}\rightarrow\text{SO}} - S_{0,\text{MO}\rightarrow\text{SO}}\, H_{0,0})^2}{H_{\text{MO}\rightarrow\text{SO,MO}\rightarrow\text{SO}} - H_{0,0}} \qquad (17)$$

where $H_{x,y}$ is the Hamiltonian between two electronic states, $S_{x,y}$ is the overlap between two electronic states, the subscript MO $\rightarrow$SO represents the electron-transferred state (between a molecular orbital of the molecule and the SOMO of the radical), and the subscript 0 represents the ground state. The denominator in eq 17 is the energy of the transferred configuration minus the energy of the ground-state configuration. At infinite separation of the two species, this is the ionization potential minus the electron affinity, IP−EA. To first order, as the two species approach each other, the ionic surface described above drops dramatically in energy from Coulombic attraction:

$$H_{\text{MO}\rightarrow\text{SO,MO}\rightarrow\text{SO}} - H_{0,0} \cong \text{IP}_{\text{MO}} - \text{EA}_{\text{SO}} - \frac{e^2}{r} \qquad (18)$$

In the numerator of eq 17, the energy of two different configurations is proportional to the overlap of those two configurations when overlap is small.[42] Thus,

$$H_{0,\text{MO}\rightarrow\text{SO}} \propto S_{0,\text{MO}\rightarrow\text{SO}} \qquad (19)$$

Furthermore, in the transfer of an electron from one species to another, the overlap of the transferred and ground state is primarily defined by the overlap of the two interacting orbitals, as expressed by the equation

$$S_{0,\text{MO}\rightarrow\text{SO}} \propto S_{\text{MO,SO}} \qquad (20)$$

Combining eqs 17−20, we find that the amount of barrier suppression due to electron delocalization is proportional to

$$D \propto \sum^{\text{OccMOs}} \frac{S_{\text{MO,SO}}{}^2}{\text{IP}_{\text{MO}} - \text{EA}_{\text{SO}} - e^2/r} \qquad (21)$$

Here we see the explicit competition between overlap and energy. The total electron delocalization is the sum of the individual interactions between the MOs of the hydrocarbon and the SOMO of OH. It is generally assumed that the HOMOs dominate the delocalization. Hence, they are defined as the frontier molecular orbitals. We will now explicitly consider lower energy orbitals with large overlap.

6.3. Calculations. We have used eq 21 along with the aforementioned ab initio studies to calculate the extent of delocalization from each orbital in the reactions under investigation. To evaluate the relative extent of delocalization, we calculate overlap integrals between the undistorted species when they have reached the distance of closest approach without geometric reorganization (i.e., where the carbon−oxygen distance is the same as at the transition state). At the end of stage 1 the overlap between the SOMO and any MO of the hydrocarbon is small, allowing for the assumption that the energy is proportional to overlap. However, at this point, our method departs from that of Fukui and Fujimoto and allows the geometry of the system to change after the initial boundary conditions to the atom transfer are established. Results are presented in Table 4. We will test against observation the hypothesis that the dominant configuration interactions at the early stage of the reaction will continue to dominate throughout the transfer stage.

TABLE 3: Activation Energies (E_a), Ground-State Dipole Attraction Energies (E^μ), and Dipole-Corrected Barrier Heights ($E_a - E^\mu$) for Methane, Ethane, Propane and Cyclopropane[a]

compound	E_a (K)	E^μ (K)	$E_a - E^\mu$ (K)
methane[b]	1860	−504	2364
ethane[c]	1026	−338	1364
propane[c]	616	−200	816
cyclopropane[c]	735	−696	1431

[a] The dipole corrections were computed from eq 6 using results from theoretical calculations (UMP2/6-31G**).

TABLE 4: Ionization Potential and the Relative Extent of Electron Delocalization with an OH Radical, as Calculated from eq 21, for the Dominant MOs of Methane, Ethane, Propane, and Cyclopropane[a]

IP (eV)	methane delocalization	IP (eV)	ethane delocalization	IP (eV)	propane delocalization	IP (eV)	cyclopropane delocalization
12.6 (HO)	6.8	11.5 (HO)	10.5	11.0 (HO)	24.5	9.8 (HO)	2.6
12.6 (HO)	2.4	11.5 (HO)	3.7	11.1 (HO*)	9.79	9.8 (HO)	2.7
12.6 (HO)	2.1	12.1	1	11.1	1	12.3 (SHO)	11.3
21.8	1	14.5	2.9	12.9	1.6	14.7	3
D_{HOMO}/D_{Total}	0.92		0.79		0.93		0.26

[a] The HOMOs for each of the species are denoted by (HO). In addition, the SHOMOs for cyclopropane are denoted by (SHO). The values for the delocalization are normalized for each compound. The fraction of delocalization that takes place in the HOMO relative to the total amount of delocalization is also given. For propane, we include the SHOMO along with the HOMO, and label it HO*. This is because these orbitals have nearly the same energy. The larger numbers indicate at which orbital the OH attacks as the reaction progresses. For methane, ethane, and propane, this is the HOMO. Cyclopropane primarily delocalizes from the SHOMOs.

TABLE 5: Ab Initio C−O and C−H Bond Distances at the Transition State, the Fractional Barrier Location Calculated from Equation 3, the Fractional Barrier Location Back-Calculated from the *r*(C−O) and *r*(C−H), the Number of Equivalent Hydrogens, and the *A*-factor at 298 K[a]

compound	r_{C-O} (Å)	r_{C-H} (Å)	ρ_{TS}/R_X ab initio	ρ_{TS}/R_X (ionic)	equivalent Hs (n_H)	A (298 K)/n_H (10^{-13} cm^3 molecule^{-1} s^{-1})
methane	2.48	1.21	−0.20	−0.23	4	6.1
ethane	2.50	1.19	−0.36	−0.29	6	13.0
propane	2.53	1.18	−0.48	−0.40	2	44.1
cyclopropane	2.44	1.19	−0.20	−0.26	6	1.3

[a] The experimental data for the OH + methane reaction is from DeMore et al.[34]

Methane and Ethane. For methane and ethane, theory predicts that the orbitals which delocalize to the largest extent during the early stages of reaction are the HOMOs. In both cases, the effective curve crossing is essentially the curve crossing determined by the HOMOs.

Propane. For propane, theory predicts that the HOMO also delocalizes to the greatest extent for an attack of an OH radical at a secondary hydrogen. The SHOMOs play a significant role in the reaction but are only 0.1 eV more stable than the HOMO, and thus, are essentially indistinguishable in energy. Again, the effective curve crossing is determined by the HOMO.

Cyclopropane. For cyclopropane, the SHOMOs dominate electron delocalization in the OH reaction. Even though these orbitals are ∼2.5 eV more stable than the HOMO, their greater spatial overlap with the SOMO of OH overwhelms the difference in energy.

It is thus not sufficient simply to define the frontier orbitals as the HOMO and SOMO (or LUMO) of a given molecule. It is clear for cyclopropane that the HOMOs play a smaller role in controlling electron delocalization than the SHOMOs. The frontier molecular orbitals are better defined as the orbitals that result in the greatest degree of delocalization. This accommodates cases where a spatially extended but energetically more stable molecular orbital can primarily determine the site (which atom and which MO) of radical attack.

6.4. Reevaluation. We can now reexamine cyclopropane in the context of our radical−molecule reactivity theory. Again, ionization potentials, electron affinities, and bond strengths are used to calculate the crossing height of the transition state using eq 2. In addition, we continue to account for the dipole-induced dipole interactions on the ground state surface (see Table 3). The ground-state attraction for cyclopropane is larger than for either ethane or propane. This is a more general indication of the location of the electron density in the molecule. In cyclopropane, electron density is focused primarily in the ring structure. This pulls electron density away from the hydrogens resulting in a greater dipole−dipole stabilization as the OH radical approaches.

Figure 9 shows a plot of activation energy versus the theoretically determined crossing height for each of the four hydrocarbons. As before, we predict the evolution of barriers for methane, ethane, and propane. Furthermore, by using the effective crossing height for cyclopropane we correctly predict that barrier as well. The crossing heights of the HOMOs and SHOMOs are weighted by the relative amount of delocalization occurring from each orbital (see Table 4). This calculation is shown graphically in Figure 6. While the role of the HOMOs is secondary, they still contribute to the total delocalization energy and lower the barrier significantly.

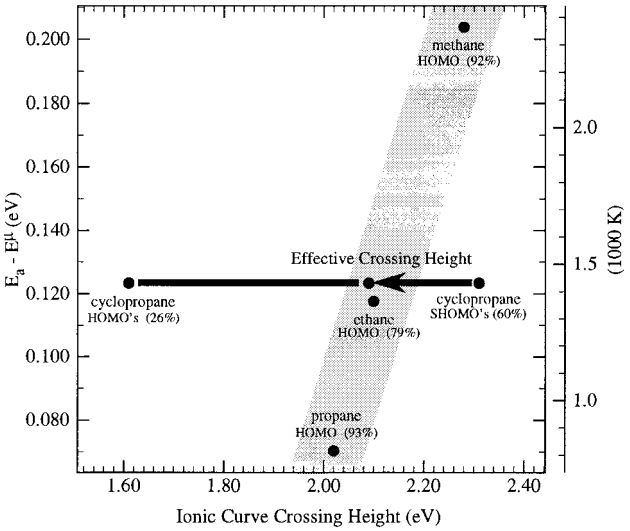

Figure 9. Activation energy (minus ground-state energy) vs crossing height. Ab initio calculations (UMP2/6-31G**) were used in calculating the crossing point. The shaded region is simply meant to guide the eye to the trend between methane, ethane, and propane, and is not an exact fit to the data. The amount of electron delocalization occurring from a particular orbital is also given. For methane, ethane, and propane, the HOMO directs the reaction. For cyclopropane, the dominant orbital is the SHOMO. Weighting the HOMOs and SHOMOs properly, an effective crossing point is determined.

6.5. Preexponential. Next we shall consider the low preexponential for the cyclopropane + OH reaction. Two aspects of the transition-state geometry change in these hydrogen atom abstraction reactions. The first is the distance between

the reactive carbon center of the alkane and the oxygen atom of OH. The second is the location of the barrier along the C−H−O hydrogen-transfer coordinate.

The C−O distance affects the preexponential factor in two ways: by directly controlling the transition-state moment of inertia and by influencing the frequencies of the loose transition-state vibrational modes. As the OH and hydrocarbon approach, free rotations of the separated species become vibrations in the transition state complex, which become more constrained as the C−O distance decreases. This is illustrated in Table 5, which includes the ab initio C−O distances (r_{C-O}) at the TS and the experimental *A*-factor divided by the number of abstractable hydrogens. The *A*-factor is the 298 K value of the preexponential portion of eq 10. The C−O distance for OH + cyclopropane is smaller than for either OH + propane or OH + ethane; this is accompanied by a correspondingly low *A*-factor.

While this partially explains the low preexponential, it does not address why the C−O distance in the OH + cyclopropane reaction is so small. The simple answer is that the reactive molecular orbital in OH + cyclopropane is less extended than in either OH + propane or OH + ethane, resulting in a lower overlap at a common point along the reaction. The balance expressed by eq 4 is therefore shifted toward a smaller interaction distance. This is verified by quantum-mechanical overlap calculations. With a lower degree of overlap, the OH must approach more closely to react. Thus, even though the electron density on the hydrogens in the SHOMOs is extended relative to the electron density in the HOMOs, it is contracted relative to the electron density on hydrogens in methane, ethane, or propane.

The location of the transition state along the H atom transfer coordinate also influences the preexponential. Greater distortion of the C−H bond is consistent with a later transition state; the hydrocarbon has to rearrange to a greater degree to reach the transition state. Our ab initio calculations show that the C−H bond distance at the transition state for OH with ethane and propane is smaller than that for OH with cyclopropane or methane (see Table 5). The greater distortion of the C−H bond in the latter two compounds corresponds with lower *A*-factors.

To compare the ab initio results with model predictions from eq 3, we first calculate the transition state location along the H atom transfer coordinate, normalized to half of the total distance traveled by the H atom ($\rho_{TS}/R_{X\ -\ \text{ab initio}}$). We then calculate this quantity from eq 3 using our ionic curve-crossing model ($\rho_{TS}/R_{X\ -\ \text{ionic}}$). The results are also shown in Table 5. Both the ionic crossing model and the ab initio transition-state locations correlate well with the experimental *A*-factors.

7. Conclusions

The transition-state energy and location are governed by a configuration interaction between the reactant ground state and one or more ionic states, described by the molecular properties of the reactants. This is confirmed by our study of OH with cyclopropane, provided the role of the second highest molecular orbitals (SHOMOs) is considered. The high barrier and low preexponential observed in the reaction of OH with cyclopropane arise because the attacking OH radical delocalizes electron density from the SHOMOs in cyclopropane. Frontier molecular orbitals are not simply the SOMO and HOMO of the two reacting species in radical−molecule reactions. They may be at the spatial and not the energetic frontier. Quantum mechanically, barrier suppression from the curve crossing depends on overlap and energy. Thus, a more suitable definition of frontier orbitals are the orbitals that dominate electron delocalization at the transition state.

Acknowledgment. The authors thank Michele Sprengnether and Ken Demerjian for helpful discussions on the reactivity of cyclopropane. We also thank Tom Hanisco for experimental assistance. This work was supported by NSF Grant 9414843 to Harvard University.

References and Notes

(1) Silver, D. M. *J. Am. Chem. Soc.* **1974**, *96*, 5959.
(2) Melissas, V. A.; Truhlar, D. J. *J. Chem. Phys.* **1993**, *99*, 1013.
(3) Steckler, R. S.; Thurman, G. M.; Watts, J. D.; Bartlett, R. J. *J. Chem. Phys.* **1997**, *106*, 3926.
(4) Pross, A. *Adv. Phys. Org. Chem.* **1985**, *21*, 99.
(5) Shaik, S. S.; Hiberty, P. C. *Adv. Quantum Chem.* **1995**, *26*, 99.
(6) Donahue, N. M.; Clarke, J. S.; Anderson, J. G. *J. Phys. Chem.* **1998**, *102*, 3923.
(7) Donahue, N. M. *J. Phys. Chem.* **1998**, *102*, Submitted.
(8) Shaik, S. S.; Hiberty, P. C.; Lefour, J. M.; Ohanessian, G. *J. Am. Chem. Soc.* **1987**, *109*, 363.
(9) Evans, M. G.; Polanyi, M. *Trans. Faraday Soc.* **1938**, *34*, 11.
(10) Marcus, R. A. *J. Chem. Phys.* **1956**, *24*, 966.
(11) Marcus, R. A. *J. Phys. Chem.* **1968**, *72*, 891.
(12) Fukui, K.; Yonezawa, T.; Haruo, S. *J. Chem. Phys.* **1952**, *20*, 722.
(13) Fleming, I. *Frontier Orbitals and Organic Chemical Reactions*; John Wiley and Sons: New York, 1976.
(14) Lowenstein, L. M.; Anderson, G. J. *J. Phys. Chem.* **1987**, *91*, 2993.
(15) Abbatt, J. P. D.; Anderson, J. G. *J. Phys. Chem.* **1991**, *95*, 2382.
(16) Abbatt, J. P. D.; Toohey, D. W.; Fenter, F. F.; Stevens, P. S.; Brune, W. H.; Anderson. G. J. *J. Phys. Chem.* **1989**, *93*, 1022.
(17) Fenter, F. F.; Anderson, J. G. *J. Phys. Chem.* **1991**, *95*, 3172.
(18) Stevens, P. S.; Anderson, J. G. *J. Phys. Chem.* **1992**, *96*, 1708.
(19) Lowenstein, L. M.; Anderson, J. G. *J. Phys. Chem.* **1984**, *88*, 6277.
(20) Rittner, E. S. *J. Chem. Phys.* **1951**, *19*, 1030.
(21) Pross, A.; Yamataka, H.; Nagase, S. *J. Phys. Org. Chem.* **1991**, *4*, 135.
(22) Sato, S. *J. Chem. Phys.* **1955**, *23*, 592.
(23) Garrett, B. C.; Truhlar, D. G. *J. Chem. Phys.* **1985**, *82*, 4543.
(24) Walsh, A. D. *Trans. Faraday Soc.* **1949**, *45*, 179.
(25) Atkinson, R. *J. Phys. Chem. Ref. Data* **1997**, *36*, 75.
(26) Abbatt, J. P. D.; Demerjian, K. L.; Anderson, J. G. *J. Phys. Chem.*, **1990**, *94*, 4566.
(27) Donahue, N. M.; Clarke, J. S.; Demerjian, K. L.; Anderson, J. G. *J. Phys. Chem.* **1996**, *100*, 5821.
(28) Donahue, N. M.; Demerjian, K. L.; Anderson, J. G. *J. Phys. Chem.*, **1996**, *100*, 7855.
(29) Rothman, L. S. *J. Quantum Spectrosc. Radiat. Transfer* **1992**, *48*, 469.
(30) Donahue, N. M.; Demerjian, K. L.; Anderson, J. G. *J. Phys. Chem.*, **1998**, *102*, 3121.
(31) Dóbé, S.; Turányi, T.; Iogansen, I.; Bérces, T. *Int. J. Chem. Kinet.* **1992**, *24*, 191.
(32) Jolly, S. G.; Paraskevopoulos, G.; Singleton, D. L. *Int. J. Chem. Kinet.*, **1985**, *17*, 1.
(33) Zetsch, C. Presented at Bunsen Colloqium, Gottingen, W. Germany, October 9, 1980. Private communication to Roger Atkinson, 1985.
(34) DeMore, W. B.; Sander, S. P.; Golden, D. M.; Hampson, R. F.; Kurylo, M. J.; Howard, C. J.; Ravishankara, A. R.; Kolb, C. E.; Molina, M. J. Chemical kinetics and photochemical data for use in stratospheric modeling. Technical Report 97-4; Jet Propulsion Laboratory: Pasadena, CA, 1997.
(35) Atkinson, R. *J. Phys. Chem. Ref. Data* Monogr. **1989**, *1*, 246.
(36) Mallard, W. G. NIST chemistry webbook. Technical Report 69; National Institute of Science and Technology, U.S. Department of Commerce: Washington, DC, 1997 (http://webbook.nist.gov).
(37) Lide, D. R.; Ed. *CRC Handbook of Chemistry and Physics*, 74th ed.; CRC Press: Boca Raton, FL, 1993.
(38) Cremer, D.; Gauss, J. *J. Am. Chem. Soc.* **1986**, *108*, 7467.
(39) Hu, W.; Rossi, I.; Corchado, J. C.; Truhlar, D. G. *J. Phys. Chem.* **1997**, *101*, 6911.
(40) Fukui, K.; Fujimoto, H. *Bull. Chem. Soc. Jpn.* **1968**, *41*, 1989.
(41) Fukui, K.; Fujimoto, H. *Bull. Chem. Soc. Jpn.* **1969**, *42*, 3399.
(42) Mulliken, R. S. *J. Chim. Phys.* **1949**, *46*, 497.